Available online at www.sciencedirect.com
SCIENCE DIRECT®
International Journal of Mass Spectrometry 229 (2003) 47–53
International Journal of Mass Spectrometry
www.elsevier.com/locate/ijms

Probing nano-environments of peptide molecules on solid surfaces by highly charged ion secondary ion mass spectrometry

Thomas Schenkel [a,*], Kuang Jen Wu [b]

[a] *E.O. Lawrence Berkeley National Laboratory, 1 Cyclotron Road, Building 5RO121, Berkeley, CA 94720, USA*
[b] *Lawrence Livermore National Laboratory, Livermore, CA 94550, USA*

Received 7 January 2003; accepted 24 January 2003

Abstract

The ability to probe the chemical composition and molecular structure of solid surfaces with nanometer scale resolution through secondary ion mass spectrometry is limited by the probe beam size and by surface erosion during analysis. High secondary ion yields following the impact of individual highly charged ions allow the application of coincidence counting techniques. Statistical analysis of secondary ion emission events gives insight on the surface chemistry of single molecules. While not a direct imaging technique, coincidence analysis allows the characterization of surfaces on a length scale of a few nanometers, well beyond limits imposed by probe beam sizes. We apply this capability to the analysis of gramicidin S and its interaction with sodium impurities and 2,5-dihydroxybenzoic acid matrix molecules.

Keywords: Peptides; Nano-environments; Solid surfaces; Secondary ion mass spectrometry; Gramicidin S

1. Introduction

The development of advanced mass spectrometry techniques has been instrumental to progress in molecular biology, biochemistry, and biological surface science. Future development of nanotechnology devices will require sensitive, specific materials analysis techniques, and methods analogous to those which are essential to high yield manufacturing of today's semiconductor devices and emerging biotechnologies [1]. However, nanometer scale research and development cannot directly employ many state-of-the-art material analysis techniques because of their limited sensitivity and/or spatial resolution.

Mass spectrometry techniques of solids, such as matrix-assisted laser desorption ionization (MALDI) and secondary ion mass spectrometry (SIMS), have advanced very rapidly in the past decade [2,3]. In MALDI, imaging of surfaces has been demonstrated, but the spatial resolution is limited by the laser spot size to a few micrometers [4].

SIMS is a mass spectrometric approach with high spatial resolution capability. In conventional SIMS, singly charged ions, such as Cs^+, O^+, and Ga^+, are used as the probe beam. Depending on the ion beam flux, SIMS techniques can be further classified as dynamic (typical ion flux $>10^{13}$ ions/cm^2/s) or static SIMS. Typically employed with magnetic sector or quadrupole mass spectrometers, dynamic SIMS is one of the most sensitive analytical technique with sub-ppb level detection sensitivity. Both dynamic and static SIMS are capable of studying solid surfaces with spatial resolutions of the orders of tens to a few hundred nanometers. The spatial resolution is determined by the spot size of the probe beam, which can be focused down to ∼100 nm for time-of-flight (TOF)-SIMS and recently developed dynamic SIMS instruments have an ultimate spatial resolution of 50 nm [5]. Even smaller probe beam sizes of only ∼10 nm are routinely achieved in focused ion beam systems. Stevie et al. have discussed sensitivity limits in FIB-SIMS [6]. Here, spatial resolution, depth resolution, and sensitivity have to be balanced for a given analytical application. For instance, the analysis of the elemental composition of a small particle on a silicon surface is affected by the fact that this particle is being eroded during analysis. Useful ion yields, i.e., the ratio of detected secondary ions per amount of sputtered material are often smaller than 0.1 and can be as small as 1E-6 for some transition metals on silicon surfaces. Techniques to increase secondary ion fractions, such as surface oxidation and ceseation, laser postionization

* Corresponding author. Fax: +1-510-486-5105.
E-mail address: T_Schenkel@LBL.gov (T. Schenkel).

1387-3806/$ – see front matter © 2003 Elsevier B.V. All rights reserved.
doi:10.1016/S1387-3806(03)00254-9

[7], use of matrix enhancement effects [8], or choice of heavy projectiles (such as C_{60} and SF_6, or ions of high-z elements, such as In and Au), have been developed. Still, the effective lateral resolution in SIMS is typically of the order of several hundred nanometers, due to the relatively low secondary ion yields in collisional sputtering by singly charged ion and the primary ion beam spot size.

We describe an approach to desorption and ionization of biomolecules using increased secondary ion yields in the interaction of slow (<2 keV/u), very highly charged ions (SHCI), such as Xe^{48+} or Au^{69+}, with solid surfaces [9,10]. Individual SHCI desorb and ionize multiple secondary ions from peptide and amino acid samples. Detection of multiple secondary ions from a single desorption event enables the application of coincidence analysis techniques. Correlations in the emission of secondary ions allow for the characterization of nano-environments of individual peptide molecules on solid surfaces [11–13].

2. Experimental and methodology

In typical SIMS instruments, secondary ion emission is a result of collisional sputtering [14]. Primary ions transfer momentum to target atoms, a (mostly linear) collision cascade ensues, while surface atoms which receive more energy than their surface binding energy are emitted into the vacuum. A fraction of the sputtered material is ionized and forms the signal in the various SIMS schemes. An alternative to collisional sputtering was discovered in the early 1970s in the interaction of swift (∼1 MeV/u) heavy ions from Tandem accelerators or from ^{252}Cf-fission sources with solid surfaces [15]. Here, sputtering is induced by electronic excitation as a result of electronic energy loss, and not by elastic collisions. This effect was soon utilized in plasma desorption mass spectrometry (PDMS). The finding of high yields of biomolecular ions spawned the idea of coincidence analysis in PDMS. Each ion emits secondary ions from a very small sample volume of ∼100 nm^3. Here, the effective emission area has been estimated to have a diameter of ∼10 nm, and the depth of origin of secondary ion was assumed to be about 1–3 nm. In PDMS, one single primary ion triggers a TOF cycle, and more than one secondary ion can be detected following the impact of only one primary ion. TOF cycles can now be stored in lists, so that they can be searched and analyzed for correlations between secondary ions. The statistical analysis of these correlations can reveal information on the nanometer scale environment of a selected species with an effective spatial resolution of only a few nanometers [16]. This effective resolution is given by the area from which the secondary ions are ejected following the impact of individual projectiles. Coincidence counting techniques can thus bridge the gap between nanometer scale imaging techniques, such as atomic force microscopy (AFM), and molecular structure techniques, such as X-ray photoelectron spectroscopy (XPS), or nuclear magnetic resonance (NMR) which probe interactions on a sub-nanometer length scale, and MS-imaging techniques which are limited to resolutions of tens of nanometers due to probe beams sizes and sample consumption effects.

In our approach, we use relatively slow, very highly charged ions (SHCI) to induce electronic sputtering and secondary ion emission. Beams of ions, like Xe^{44+} and Au^{69+}, can be extracted from an electron beam ion trap (EBIT) [17]. EBITs are relatively compact sources for highly charged ions (compared to Tandem accelerators), and beams of SHCI can be focused to sub-micron spot sizes [18] to allow for a combination of course imaging and nano-scale analysis (in contrast to ions from fission fragment sources).

In Fig. 1, we show positive secondary ion yields (in units of detected secondary ions per incident ion) of gramicidin S molecules from a gramicidin S sample as a function of the potential energy of SHCI. The overall detection efficiency of the short linear TOF spectrometer with annular microchannelplate detector of ∼0.15 is not included in these yields [9]. Details of the experimental setup have been described in ref. [9,10]. The target consisted of gramicidin S with 2,5-dihydroxybenzoic acid (DHB) mixed in a ratio of about 1:1000. Analyte and matrix were mixed in water and a droplet of the solution was allowed to dry on a native oxide surface of a silicon wafer. Secondary ion yields are known to depend sensitively on the surface composition of samples. Yields of detected ions in repeated experiments with gramicidin S samples showed variations of the order of 50%, but trends, such as scaling with the projectile charge state, were very reproducible. Increasing the charge state or the potential energy of xenon and gold projectiles, we find a near linear increase of positive secondary ion yields from the analyte, $[M + H]^+$, as a function of potential energy of projectiles. The increase by a factor of 20 when using Au^{69+} as compared to Xe^{22+} underscores the advantage of the use of very highly charged ions for analysis of biological compounds.

Electronic sputtering in the interaction of slow ($v < v_0 =$ 2.1E-6 m/s) highly charged ions results from the fast deposition of internal electronic excitation energy of the projectiles when they impinge on a surface. SHCI, like Xe^{44+}, deposit a potential energy of 50 keV within about 10 fs close to the surface. Secondary electrons are emitted (about 50 for Xe^{44+} on SiO_2 films [19]) and surface atoms and molecules are excited by cascades of electronic transitions. Shock waves following Coulomb explosions of highly ionized nanometer scale volumes have been suggested as the driving mechanism for the emission of intact biomolecules [9,11,20]. Atomic ions are emitted mostly from the center of the interaction region, while large molecules stem from areas with lower ionization density. The kinetic energy of projectiles plays only a secondary role in electronic sputtering by SHCI, and gramicidin S ion yields were the same for Xe^{44+} projectiles with 10 and 220 keV [9,10]. Fragmentation, as measured by the ratio of intact analyte ions to carbon ions is slightly increased for higher charge states. Data for damage cross-sections and static SIMS dose limits for SHCI are not

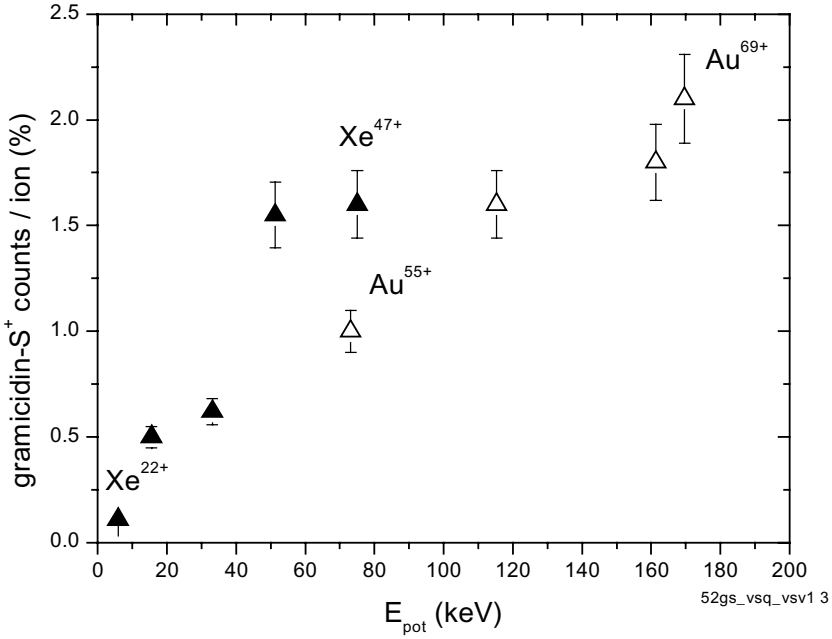

Fig. 1. Positive secondary ion counts per incident projectile vs. potential energy of projectiles. The kinetic energy of projectiles varied as 5.4 kV q.

yet available [10]. Detailed mechanisms describing the coupling of electronic excitation (potential energy) from SHCI to the motion of atoms and large molecules are still a matter of controversial debate [9,21,22].

The analysis of coincidences in secondary ion emission becomes possible when two conditions are satisfied: Secondary ions must be collected following the impact of one projectile, and the probability for detection of two secondary ions from one impact has to be large compared to the number of impact events and compared to background.

Both conditions are satisfied in electronic sputtering by SHCI [9–13] and also for swift heavy ions, such as fission fragments [15,16,23]. For SHCI, the average number of detected secondary ions per impact event can be larger than one [19]. It has to be considered that this yield includes all secondary ion species. A yield of 0.01 for two selected secondary ions results in a combined probability of about 10^{-4} for the uncorrelated detection of both secondary ions following a single impact event. Assuming the accumulation of spectra over a few million impact events, this would produce a useful peak in the analyzed data. Fig. 2 shows a schematic of the coincidence analysis experiment.

Individual SHCI impinge on a sample and trigger TOF cycles. In negative (positive) polarity, detection of secondary electrons (protons) starts the TOF cycle [9,11]. Several secondary ions are emitted, and coincidence analysis is practical when at least two secondary ions are detected with a combined probability of 10^{-4}. Storing the data from individual TOF cycles separately ("list mode") rather than summing them up to built a spectrum in the usual histogram mode, allows the selection of TOF cycles where a specific secondary ion was detected. Adding only TOF cycles in which the selected ion was detected results in coincidence spectra, which contain only secondary ions that were emitted in impact events in which the selected species was also detected. Each projectile forms secondary ions from a surface area with an estimated size of only a few tens of nanometers, and the correlations therefore contain information about the local chemical composition.

The correlation coefficient, $C(\mathrm{A},\mathrm{B})$, gives a measure for the probability to detect a secondary ion B in coincidence with ion A [16]:

$$C(\mathrm{A},\mathrm{B}) = \frac{P(\mathrm{A},\mathrm{B})}{P(\mathrm{A})\,P(\mathrm{B})} \tag{1}$$

Here, $P(\mathrm{A})$ and $P(\mathrm{B})$ are the probabilities for the detection of secondary ions A and B independently in all impact events. $P(\mathrm{A},\mathrm{B})$ is the probability for detection of A and B in the same impact event. For $C(\mathrm{A},\mathrm{B}) > 1$, it is more likely to

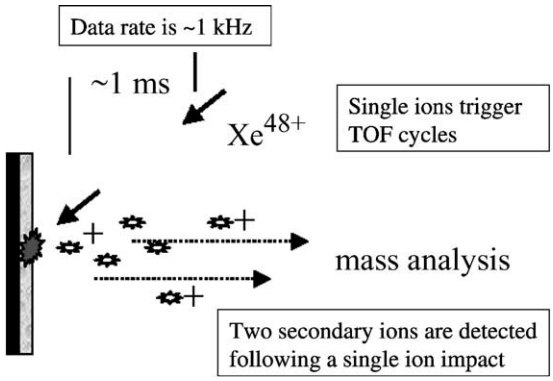

Fig. 2. Schematic of HCI-SIMS coincidence counting experiment.

detect A when B is also present. For example, emission of ions from the copper isotopes 63 an 65 is very much correlated ($C > 5$) when the copper is present as copper clusters on a silicon wafer, while emission of copper and silicon ions is not correlated [11,12].

SIMS with coincidence counting offers the possibility for the study of interaction and bonding of peptides and proteins in the solid phase where weak (1–5 kcal/mol), non-covalent interactions are operative. Weak non-covalent interactions are difficult to detect and it is hard to determine regions of interaction. Mass spectrometry techniques to aid in the understanding of where and how small molecules bind, e.g., to the surface of proteins, are highly desirable for many applications, such as the development of biological sensors based on molecular recognition principles.

We now apply SIMS with coincidence counting to a study of gramicidin S, a cyclic decapeptide antibiotic, and its interaction with sodium and a DHB matrix.

3. Results and discussion

Two gramicidin S samples were prepared. The first sample consisted of a layer of neat gramicidin S molecules deposited on a clean Si wafer surface. The second sample involved embedding gramicidin S in a solid phase matrix compound DHB with a nominal concentration ratio of 1:1000. Consequently, the surface concentration ratio of gramicidin S to DHB is approximately 1:100 with the assumption of homogeneous mixture. Samples were not desalted and sodium was present in the solid mixture.

The positive ion HCI-SIMS spectra obtained from the neat gramicidin S and gramicidin S/DHB mixture are shown in Fig. 3. Both spectra showed the presence of a protonated $[M+H]^+$ peak along with a Na cationized peak $[M+Na]^+$. The gramicidin S signal intensity is significantly higher from the gramicidin S/DHB mixture. Projectiles were Xe^{44+} ions with a kinetic energy of 20 keV. The ion yields or the number of analyte ions generated per primary ion impact were 1.2 and 4% for neat gramicidin S and gramicidin S/DHB, respectively. This represents a factor of 3 increase in ion yield albeit the gramicidin S surface concentration is approximately 100 times less for the gramicidin S/DHB mixture. The presence of the MALDI matrix DHB clearly enhances the ejection and ionization of gramicidin S molecules. Such ionization enhancement effects with various matrix molecules, such as DHB, cocaine, and others, have been reported previously for conventional static SIMS [8]. It is intriguing that the MALDI matrix DHB exhibits strong secondary ion enhancement following excitation by highly charged ions. This finding raises fundamental questions on the function of matrix molecules in sputtering and ion formation processes. For example, whether these analyte ions existed in the solid sample mixture as pre-formed ions or whether they formed above the surface after neutral molecules were emitted into the vacuum. The mechanism for ionization enhancement is most likely short range, so that only the nearest neighboring molecules surrounding the analyte contribute to enhanced ion yields. Both the binding of matrix and analyte molecules in the solid and collisional ion formation processes have been suggested to play important roles for ion yield enhancements in MALDI and matrix enhanced SIMS [8,24].

Fig. 4a–c show positive secondary ion spectra obtained from a gramicidin S/DHB mixture sample. The probe beam was Au^{69+} with a kinetic energy of 140 keV. Spectra were taken with a short, linear TOF spectrometer described in ref.

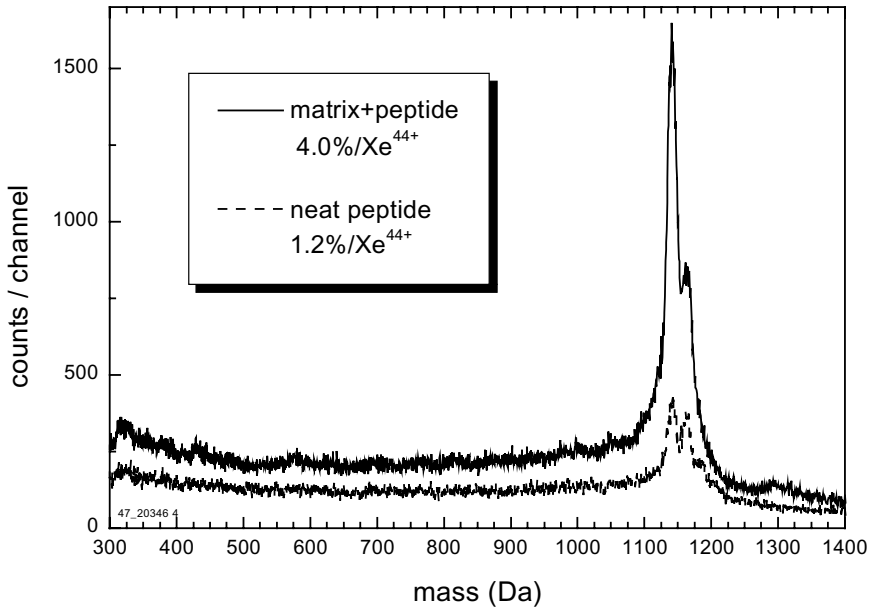

Fig. 3. Section of a TOF-SIMS spectrum from a neat gramicidin S sample, and a sample where gramicidin S molecules were embedded in a 2,5-dihydroxybenzenzoic acid matrix. Primary ions were Xe^{44+} with a kinetic energy of 20 keV.

[20]. The gramicidin S ions are observed in two ionization forms: protonated ions $[M+H]^+$ and a weak sodium cationized peak $[M+Na]^+$. The protonation of gramicidin S is attributed to the proton donation from the adjacent molecules, such as DHB. The presence of $[M + Na]^+$ peaks suggests strong interactions between analyte and sodium.

Analyzing coincidences of secondary ions permits the extraction of information on chemical composition and molecular interactions on a length scale of about 1–10 nm. A coincidence analysis spectrum requiring DHB is shown in Fig. 4a. The spectrum is the summation of a subset of mass spectra where DHB ($m/q = 154$) ions were detected. For comparison, the total ion spectrum is shown in the upper panel. Notice that the $[M + H]^+$ ions are present in the coincidence spectrum, while the intensity of $[M + Na]^+$ ions is just above background. Emission of $[M + Na]^+$ is not correlated with the emission of DHB molecular ions.

A fragment of the matrix molecule DHB, $[DHB–OH]^+$, representing the loss of a hydroxyl group is often observed in the mass spectrum with m/z value at 137. The coincidence spectrum requiring the presence of $m/q = 137$ units is shown in Fig. 4b. It is important to note that both $m/q =$

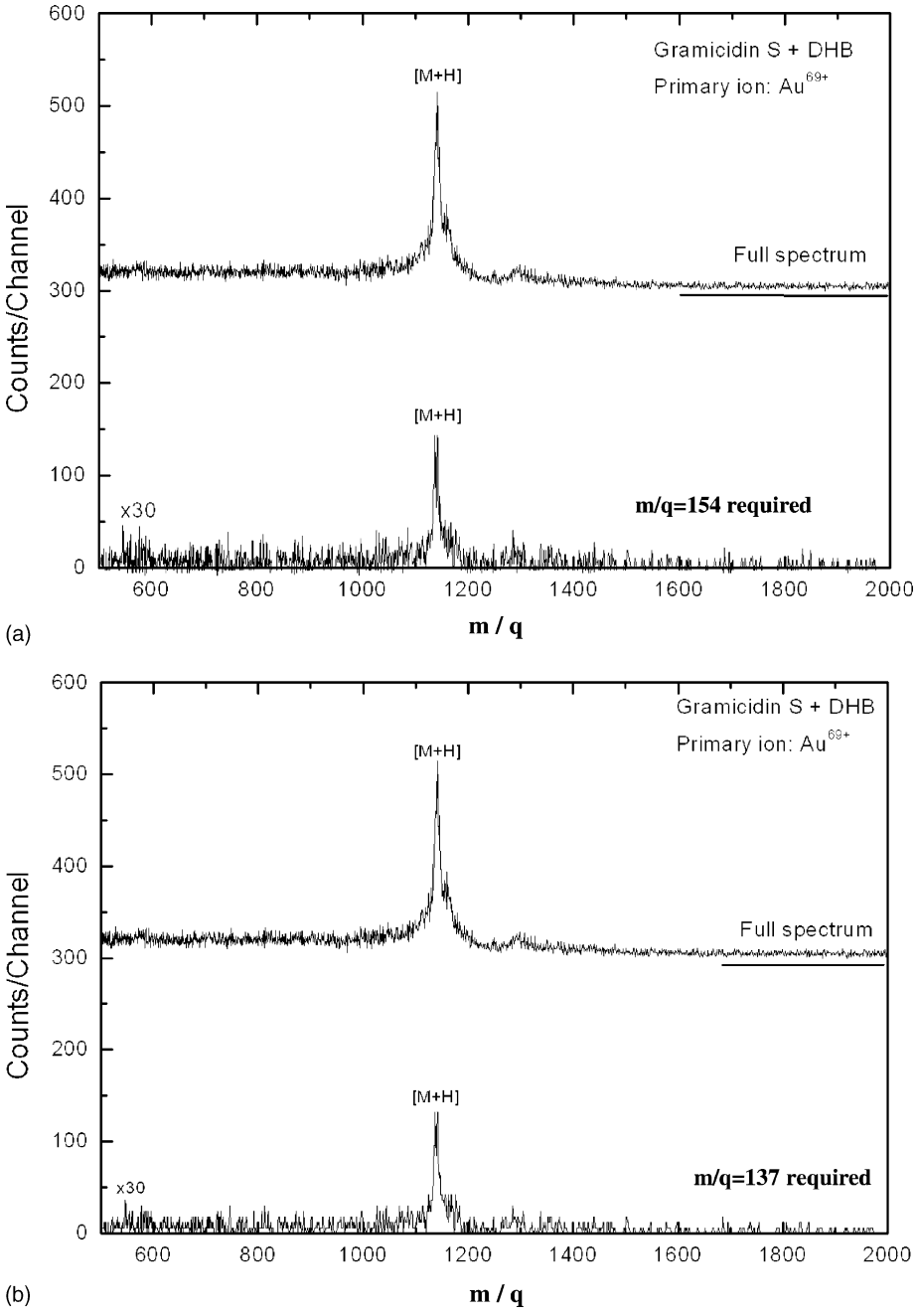

Fig. 4. HCI-SIMS spectra from gramicidin S in a 2,5-dihydroxybenzoic acid (DHB) matrix, and spectra resulting from coincidence analysis where counts from only those TOF cycles are added which contained ions of (a) mass 154 units (DHB), (b) mass 137 units (DHB–OH), and (c) mass 23 units (Na^+).

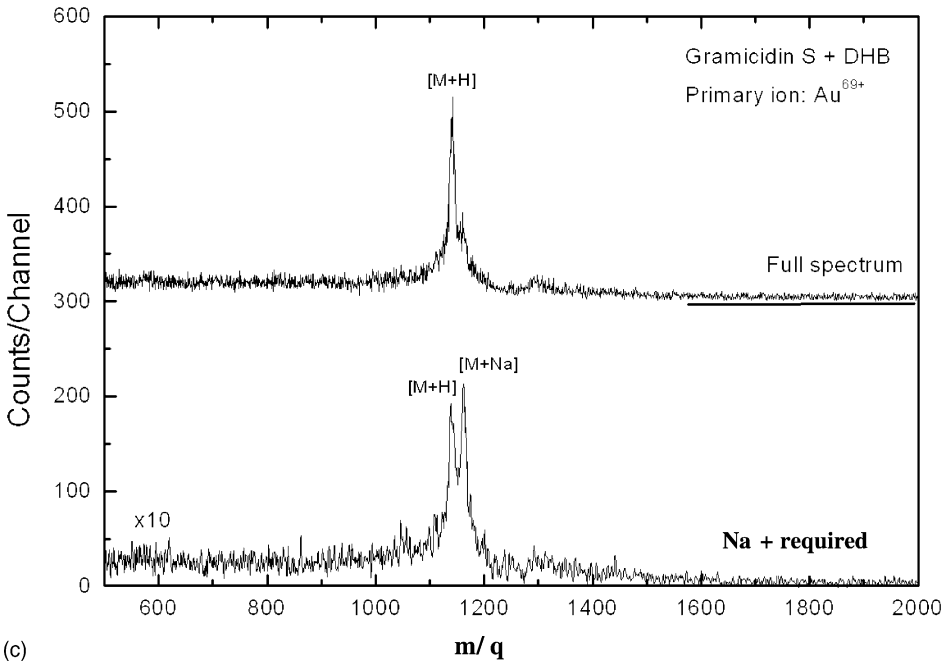

Fig. 4. (*Continued*).

154 and 137 coincidence spectra showed correlation to the protonated ion $[M + H]^+$ only. Additionally, the intensity of $[M + H]^+$ peaks in both spectra is comparable, indicting a similar degree of correlation of gramicidin S ions to these matrix ions. This also indicates that the fragmentation of DHB molecules by the loss of a hydroxyl group, which conceivably could provide extra protons available for the ionization of analyte ions, does not play a critical role in analyte ionization processes. Although gramicidin S molecules are surrounded by the DHB molecules and coincidence spectra showed correlation between these two molecules, this correlation is very weak. Hence, we conclude that there is only a weak interaction between gramicidin S and DHB.

The second ionization form is $[M+Na]^+$. It is known that gramicidin S interacts strongly with Na, and we can expect a strong correlation between Na and the Na adduct $[M+Na]^+$ ion yield. Fig. 4c shows the full HCI-SIMS spectrum (top) and the Na coincidence spectrum (bottom). When summing only emission events where a Na^+ ion was also detected, the resulting spectrum shows a relatively stronger $[M + Na]^+$ peak and only a weaker $[M + H]^+$ peak was observed. The significant reduction in $[M + H]^+$ peak intensity confirms that Na is weakly correlated to the $[M+H]^+$ ions, indicating a minimal contribution to the formation of $[M + H]^+$ ions. Emission of Na^+ and $[M + Na]^+$ are highly correlated as evidenced by the strong intensity of $[M + Na]^+$ peak. The correlation coefficient for $[M+Na]^+$ and Na^+ ions is 5, i.e., the probability for the detection of $[M+Na]^+$ together with Na^+ is five times larger than the product of the probabilities for detection of $[M + Na]^+$ and Na^+ alone. This shows that sodium is mostly responsible for the $[M + Na]^+$ formation and there is strong interaction between gramicidin S molecules and sodium. It also shows that at least two sodium atoms from NaCl molecules surround individual gramicidin S molecules. This example demonstrates that coincidence analysis in SIMS with high ion yields opens the possibility of probing molecular interactions.

4. Conclusion and outlook

Probing the interaction of DHB, gramicidin S, and sodium is a proof-of-principle example of SIMS with coincidence counting. The analysis of coincidences in secondary ion mass spectra reveals information on the interaction of molecules on a length scale of 1–10 nm. This information is extracted through statistical analysis and is thus less intuitive than results from direct imaging. Ideally, imaging on a length scale of a few hundred nanometers would be combined with coincidence analysis. Recent studies indicate that the required focused beams of highly charged ions are within reach [17].

Acknowledgements

This work was performed under the auspices of the U.S. Department of Energy by E.O. Lawrence Berkeley National Laboratory and Lawrence Livermore National Laboratory under Contracts No. DE-AC03-76SF00098 and No. W-7405-ENG-48, respectively. This work was in part supported by an SBIR grant from the U.S. Department of Commerce (#50-DKNB-9-90088).

References

[1] B.D. Rattner, A.S. Hoffman, F.J. Schoen, J.E. Lemons (Eds.), Biomaterials Science, Academic Press, San Diego, 1996.
[2] F. Hillenkamp, M. Karas, R.C. Beavis, B.T. Chait, Anal. Chem. 63 (1991) 1193A.
[3] G. Gillen, R. Lareau, J. Bennett, F. Stevie (Eds.), Proceedings of the Biannual International Conference on Secondary Ion Mass Spectrometry, e.g., SIMS XI, Wiley, Chichester, 1998.
[4] P.J. Todd, T.G. Schaaff, P. Chaurand, R.M. Caprioli, J. Mass Spectrom. 36 (2001) 355.
[5] P. Hoppe, New Astronomy Rev. 46 (2002) 589.
[6] F. Stevie, et al., J. Vac. Sci. Technol. B17 (1999) 2476.
[7] C. He, J.N. Basler, C.H. Becker, Nature 385 (1997) 797.
[8] K.J. Wu, R.W. Odom, Anal. Chem. 68 (1996) 873.
[9] (a) T. Schenkel, A.V. Hamza, A.V. Barnes, D.H. Schneider, Prog. Surf. Sci. 61 (1999) 23;
(b) T. Schenkel, A.V. Hamza, A.V. Barnes, M.W. Newman, T. Niedermayr, M. Hattass, J.W. McDonald, D.H. Schneider, K.J. Wu, R.W. Odom, Phys. Scripta T80 (1999) 73.
[10] T. Schenkel, in: P. Chakraborty (Ed.), Ion Beam Analysis of Surfaces and Interfaces of Condensed Matter Systems, Nova, New York, 2003.
[11] T. Schenkel, M.W. Newman, T.R. Niedermayr, G.A. Machicoane, J.W. McDonald, A.V. Barnes, A.V. Hamza, J.C. Banks, B.L. Doyle, K.J. Wu, Nucl. Instrum. Methods B 161–163 (2000) 65.
[12] T. Schenkel, K.J. Wu, J. Li, N. Newman, A.V. Barnes, J.W. McDonald, A.V. Hamza, J. Vac. Sci. Technol. B17 (1999) 2331.
[13] A.V. Hamza, T. Schenkel, A.V. Barnes, D.H. Schneider, J. Vac. Sci. Technol. A17 (1998) 303.
[14] P. Sigmund, Nucl. Instrum. Methods B 27 (1987) 1.
[15] (a) R.D. Macfarlane, D.F. Torgerson, Science 191 (1976) 920;
(b) R.D. Macfarlane, Anal. Chem. 55 (1983) 1247.
[16] (a) M.A. Park, K.A. Gibson, L. Quinones, E.A. Schweikert, Science 248 (1990) 988;
(b) E.F. da Silveira, et al., Surf. Sci. 408 (1998) 28.
[17] T. Schenkel, A. Persaud, A. Kraemer, J.W. McDonald, J.P. Holder, A.V. Hamza, D.H. Schneider, Rev. Sci. Instrum. 73 (2002) 663.
[18] T. Schenkel, A. Persaud, S.J. Park, J. Meijer, J.R. Kingsley, J.W. McDonald, J.P. Holder, J. Bokor, D.H. Schneider, J. Vac. Sci. Technol. B20 (2002) 2816.
[19] T. Schenkel, A.V. Barnes, M.A. Briere, A. Hamza, A. Schach von Wittenau, D. Schneider, Nucl. Instrum. Methods B 125 (1997) 153.
[20] (a) K. Wien, Rad. Eff. Def. Solids 109 (1989) 137;
(b) R.E. Johnson, B.U.R. Sundqvist, Physics Today, March 1992, p. 28.
[21] (a) I.S. Bitensky, E.S. Parilis, Nucl. Instrum. Methods Phys. Res. B 21 (1987) 26;
(b) H. Winter, F. Aumayr, Phys. Scripta T92 (2001) 15.
[22] T. Schenkel, A.V. Barnes, A.V. Hamza, D.H. Schneider, Eur. Phys. J. D1 (1998) 297, 302.
[23] C.W. Diehnelt, R.D. English, M.J. Van Stipdonk, E.A. Schweikert, Nucl. Instrum. Methods B 193 (2002) 883.
[24] R. Zenobi, R. Knochenmuss, Mass Spectrom. Rev. 17 (1998) 337.